

Photoactivation of the 391.69 keV isomer state of ^{113m}In by the $(\gamma, 2n)$ reaction

Z. Medic ¹, M. Krmar,² N. Jovancevic ², D. Maletic ¹, Y. Teterev ³, and S. Mitrofanov ³

¹*Institute of Physics, Belgrade 11000, Republic of Serbia*

²*Physics Department, Faculty of Sciences, University of Novi Sad, Novi Sad 21000, Republic of Serbia*

³*Flerov Laboratory of Nuclear Reactions, Joint Institute for Nuclear Research, Dubna 141980, Russia*



(Received 28 September 2023; accepted 26 January 2024; published 12 March 2024)

Natural indium targets were exposed to high-energy bremsstrahlung radiation, from 9 MeV to 23 MeV. Using the measured γ spectra, the yield ratio of ^{113m}In and ^{115m}In was determined. It was checked to what extent the measured values of the yield ratio can be reproduced using the existing experimental data of cross sections of relevant photonuclear reactions, as well as cross sections obtained by TALYS calculations. The measured reaction yield ratio was used to reconstruct the energy differential cross section of $^{115}\text{In}(\gamma, 2n)^{113m}\text{In}$ using the unfolding procedure.

DOI: [10.1103/PhysRevC.109.034607](https://doi.org/10.1103/PhysRevC.109.034607)

I. INTRODUCTION

Photonuclear reactions are appealing phenomena that occur when external radiation interacts with the nucleus through electromagnetic forces, without involving the nuclear force. The theoretical understanding of this phenomenon, particularly the giant dipole resonance (GDR), has been relatively successful [1]. As experimental techniques advanced, systematic data collection was initiated, primarily focusing on (γ, n) nuclear reactions. In these reactions, the nucleus releases excitation energy by emitting one neutron after interacting with electromagnetic radiation. A comprehensive systematic data set [2,3] exists in the form of energy differential cross sections for these reactions. However, there is a scarcity of experimental data for $(\gamma, 2n)$ reactions, and for (γ, xn) reactions involving more than two emitted neutrons. Energy differential cross sections are only available through theoretical estimation. Numerical codes, such as TALYS 1.9 [4], have been developed to estimate cross sections for various nuclear reactions based on theoretical assumptions.

Indium photoactivation, involving (γ, n) as well as (γ, γ') reactions, has been a subject of extensive research. Despite this, uncertainties persist regarding the photoexcitation of the ^{115m}In isomeric state, leading to variations in measured cross sections among different authors. To date, only one set of experimental measurements for the energy differential cross section of the $^{115}\text{In}(\gamma, 2n)^{113m}\text{In}$ reaction has been published, dating back over 60 years [5]. Cross-section estimates for this reaction obtained using the TALYS 1.9 code differ slightly depending on the choice of functions describing the level density and radiation strength function.

This paper aims to compare the relative yields of the $^{115}\text{In}(\gamma, 2n)^{113m}\text{In}$ reaction measured at several energies with calculated ones. Available cross-sectional data, both experimental and estimated using TALYS 1.9 were used. Furthermore, we will attempt to reconstruct the energy differential cross section for this reaction based on unfolding technique.

II. METHOD

Natural indium consists of two isotopes, ^{115}In (95.7%) and ^{113}In (4.3%). In high-energy photon beams with energies below 16.3 MeV, the only method to excite ^{113}In to its long-lived excited state at 391.69 keV is through the $^{113}\text{In}(\gamma, \gamma')^{113m}\text{In}$ reaction. However, when the photon energy exceeds 16.3 MeV, the $^{115}\text{In}(\gamma, 2n)^{113m}\text{In}$ nuclear reaction becomes dominant. Consequently, the formation of ^{113m}In can occur via two distinct reactions, and the total activity produced during irradiation is a result of the combined contribution of both of them. The probabilities of these mentioned reactions are determined by cross sections, denoted as $\sigma_{\gamma, 2n}^{115}$ for $^{115}\text{In}(\gamma, 2n)^{113m}\text{In}$ and $\sigma_{\gamma, \gamma'}^{113}$ for $^{113}\text{In}(\gamma, \gamma')^{113m}\text{In}$, where the atomic number of the parent nuclei is indicated as a superscript. The yield of ^{113m}In can be expressed as follows:

$$Y(^{113m}\text{In}) = \frac{m_t}{M} N_A \left[0.957 \int_{E_t^{\gamma, 2n}}^{E_{\max}} \sigma_{\gamma, 2n}^{115}(E) \Phi(E) dE + 0.043 \int_{E_t^{\gamma, \gamma'}}^{E_{\max}} \sigma_{\gamma, \gamma'}^{113}(E) \Phi(E) dE \right], \quad (1)$$

where the mass of the exposed target is denoted by m_t , M is the mass number and N_A is Avogadro's number. $E_t^{\gamma, 2n}$ and $E_t^{\gamma, \gamma'}$ are energy thresholds for the $^{115}\text{In}(\gamma, 2n)^{113m}\text{In}$ and $^{113}\text{In}(\gamma, \gamma')^{113m}\text{In}$ reactions, respectively. The maximum energy of photons is denoted by E_{\max} , and the flux of incident photons is $\Phi(E)$. The integrals in Eq. (1) are commonly referred to as saturation activity.

After irradiation, the γ spectra of the indium target should be recorded. The yield of ^{113m}In can then be calculated by analyzing the intensity of the 391.69 keV γ line:

$$Y(^{113m}\text{In}) = \frac{N_\gamma(391)\lambda_{113}}{\epsilon(391)p_\gamma^{391} e^{-\lambda_{113}\Delta t} (1 - e^{-\lambda_{113}t_{\text{irr}}})(1 - e^{-\lambda_{113}t_m})}, \quad (2)$$

where N_γ is detected number of 391.69 keV γ photons, λ_{113} is decay constant of ^{113m}In , ϵ is the detector's efficiency at the observed energy. The quantum yield of the 391.69 keV transition is denoted by p_γ^{391} , and t_{irr} , and t_m indicate how long the irradiation and measurement of the activated sample lasted, while Δt , so-called cooling time indicates how much time passed from the end of the irradiation to the beginning of the measurement. The above equation can be found in publications of other authors in a slightly different form [6].

The processing of the data obtained in the experiment can be significantly simplified by observing the relative yield of ^{113m}In . The optimal procedure involves normalizing the yield of ^{113m}In with the yield of some other isotope obtained from the same target and measured at the same time. The most suitable candidate for normalization is ^{115m}In , which forms through the photoactivation of the isomer state at 336.24 keV. The yield ratio of ^{113m}In and ^{115m}In can be expressed as follows:

$$\frac{Y(^{113m}\text{In})}{Y(^{115m}\text{In})} = \frac{\int_{E_{\text{th}}^{\gamma,2n}}^{E_{\text{max}}} \sigma_{\gamma,2n}^{115}(E)\Phi(E)dE}{\int_{E_{\text{th}}^{\gamma,\gamma'}}^{E_{\text{max}}} \sigma_{\gamma,\gamma'}^{115}(E)\Phi(E)dE} + \frac{0.043 \int_{E_{\text{th}}^{\gamma,\gamma'}}^{E_{\text{max}}} \sigma_{\gamma,\gamma'}^{113}(E)\Phi(E)dE}{0.957 \int_{E_{\text{th}}^{\gamma,\gamma'}}^{E_{\text{max}}} \sigma_{\gamma,\gamma'}^{115}(E)\Phi(E)dE}. \quad (3)$$

The cross section for the $^{115}\text{In}(\gamma, \gamma')^{115m}\text{In}$ reaction is denoted as $\sigma_{\gamma,\gamma'}^{115}$. Experimental data for this cross section, which are not always consistent, can be found in databases [7], along with the cross section for the $^{113}\text{In}(\gamma, \gamma')^{113m}\text{In}$ reaction.

The advantage of this approach is that no absolute photon flux is necessary. For the numerical procedure, only the shape of the photon spectra is required. It can be derived by simulation for a known geometry of bremsstrahlung production.

The experimentally obtained yield ratio of ^{113m}In to ^{115m}In can be expressed as follows:

$$\frac{Y(^{113m}\text{In})}{Y(^{115m}\text{In})} = \frac{N_\gamma(391) \lambda_{113} \epsilon(336) p_\gamma^{336}}{N_\gamma(336) \lambda_{115} \epsilon(391) p_\gamma^{391}} \times \frac{e^{-\lambda_{115}\Delta t} (1 - e^{-\lambda_{115}t_{\text{irr}}})(1 - e^{-\lambda_{115}t_m})}{e^{-\lambda_{113}\Delta t} (1 - e^{-\lambda_{113}t_{\text{irr}}})(1 - e^{-\lambda_{113}t_m})}. \quad (4)$$

All quantities in Eq. (4) with the “336” index or “115” subscript have the same meaning as explained in Eq. (2), describing the decay of ^{115m}In . Importantly, this approach does not require the absolute value of the detector efficiency; instead, relative efficiency can be used.

Using the measured intensities of the corresponding γ lines in collected γ spectra, the experimental values of the $Y(^{113m}\text{In})/Y(^{115m}\text{In})$ yield ratio can be determined [Eq. (4)]. With the estimated shape of the photon bremsstrahlung spectra $\Phi(E)$, the same $Y(^{113m}\text{In})/Y(^{115m}\text{In})$ yield ratio can be obtained from Eq. (3), using theoretical or available experimental cross sections for observed photonuclear reactions. There are two ways in which Eq. (3) and Eq. (4) can be applied in the context of studying the photoactivation of ^{113}In :

- (1) For several selected energies of the photon beam (denoted as E_{max}), which are higher than the

threshold for the $(\gamma, 2n)$ reaction, the yield ratios of $Y(^{113m}\text{In})/Y(^{115m}\text{In})$ can be determined using the obtained γ spectra. Numerical codes like TALYS 1.9 can provide estimates of the cross sections for all three reactions in Eq. (3). Using the known experiment geometry, the shape of the photon flux $\Phi(E)$ can be obtained by simulation, as well as the integrals (saturation activities) appearing in Eq. (3). Based on calculated $Y(^{113m}\text{In})/Y(^{115m}\text{In})$ yield ratios, conclusions can be drawn regarding the model assumptions' capacity (level density and radiation strength function) to reproduce the experimental yields.

- (2) Cross sections corresponding to the three saturation activities in Eq. (3) can be found in databases. It can be used to estimate the yield ratio and compare it with the obtained measurement results, providing an additional assessment of the relevance of the existing experimental values of the observed reactions' cross sections. It should be noted that for $^{115}\text{In}(\gamma, \gamma')$ and $^{113}\text{In}(\gamma, \gamma')$, measurements of cross sections were not conducted in the entire energy region covered by this experiment.
- (3) If the yield ratio of $Y(^{113m}\text{In})/Y(^{115m}\text{In})$ is determined for several different energies above the 16.3 MeV threshold, the cross section for the $^{115}\text{In}(\gamma, 2n)^{113m}\text{In}$ reaction can be determined using a suitable unfolding algorithm. It is noteworthy that only one available result of the $^{115}\text{In}(\gamma, 2n)^{113m}\text{In}$ cross-section measurement dates back more than 60 years ago [5].

III. MEASUREMENTS

A. Irradiation

The irradiation was carried out using MT25 Microtron [8] located in Flerow Laboratory of Nuclear reactions, JINR, Dubna. Technical details concerning used device and irradiation procedure are described in couple of previous publications [9].

Indium disks were exposed to bremsstrahlung with endpoint energies from 9 MeV to 23 MeV in steps of 1 MeV. For the photon production a 1 mm thick tungsten radiator was used. The distance between the tungsten radiator and an indium disk was 136 cm. The scheme of the experimental setup is presented in Fig. 1.

When high-energy photons interact with a tungsten target, fast neutrons are inevitably produced. The influence of and ^{113m}In production by inelastic neutron scattering, $^{115}\text{In}(n, n')^{115m}\text{In}$ and $^{113}\text{In}(n, n')^{113m}\text{In}$, especially at high photon energies was minimized by placing the indium disks at the center of a water container with a diameter of 18 cm. In this manner, fast neutrons resulting from photonuclear reactions in tungsten were thermalized. The number of neutrons created is highly dependent on the maximum bremsstrahlung energy. It was observed that the saturation activity of ^{116m}In , produced by neutron capture, was about 130 times higher at a photon energy of 23 MeV than at the endpoint energy of 10 MeV when indium targets were placed in water. In order to check the degree of thermalization of neutrons, two

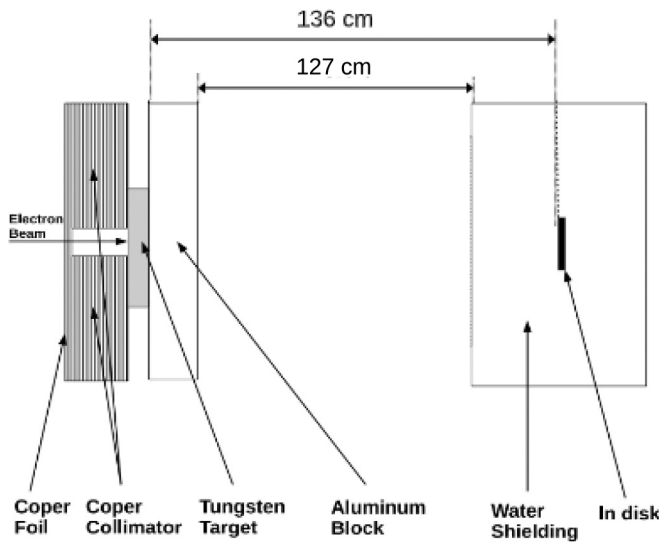


FIG. 1. Geometry of experimental setup (not in scale).

measurements were performed at energies of 21 MeV and 23 MeV where the indium samples were exposed in a photon beam with and without a water moderator. At both energies, the saturation activity of ^{116m}In was ten times higher when the indium disk was in water. Significantly lower difference in ^{115m}In saturation activities between exposures with and without water surrounding the indium samples was observed. A 14.5% higher saturation activity of ^{115m}In was observed when the disk was exposed outside the water container at a maximum photon energy of 23 MeV compared to the saturation activity when the disk was positioned inside the water container. At an energy of 21 MeV, that difference was 16.8%.

In order to verify the possible influence of (n, n') reactions on the excitation of the observed isomeric states, a GEANT simulation was performed for the geometry shown in Fig. 1 and 50×10^6 incident electrons with an energy of 23 MeV. The total number of photons and neutrons in the energy region of interest, above the energy of metastable state of ^{115m}In , at the site of the indium cylinder was monitored. It was found that the ratio of the number of photons to the number of neutrons is 1.03×10^5 . The same calculation was repeated for 18 MeV and it was obtained that the ratio of photons to neutrons is even higher and is equal to 3.54×10^5 . Although the cross section for the (n, n') reaction is almost three orders of magnitude higher than the cross section for (γ, γ') reactions, the large difference in the number of protons and neutrons gives a good basis for assuming that the inelastic scattering of neutrons does not lead to a significant excitation of the observed isomer. It was also estimated that the saturation activity ^{115m}In should be about 15% lower in the case when the activation is performed by a 23 MeV bremsstrahlung beam that is attenuated in a 9 cm thick layer of water.

Another possible way of exciting the isomeric state of ^{115}In by (γ, γ') reaction was verified. There is a possibility that the photoneutrons created in the water and the indium sample

TABLE I. Irradiation characteristics for each indium disk: m : mass of disk; E_{max} : bremsstrahlung endpoint energy; Q : integral number of electrons striking tungsten target; t_{irr} : time of irradiation.

Disk No.	m [g]	E_{max} [MeV]	Q [mAs]	t_{irr} [s]
1	0.7711	9.00(5)	7000	1800.0(5)
2	0.6317	10.00(5)	6000	1800.0(5)
3	0.6813	11.00(5)	6000	1800.0(5)
4	0.6545	12.00(5)	6000	1800.0(5)
5	0.6533	13.00(5)	2700	1800.0(5)
6	0.6317	14.00(5)	2767	1800.0(5)
7	0.6685	15.00(5)	4000	1800.0(5)
8	0.6685	16.00(5)	4000	1800.0(5)
9	0.6813	17.00(5)	2700	1680.0(5)
10	0.6531	18.00(5)	2700	960.0(5)
11	0.6758	19.00(5)	2700	2100.0(5)
12	0.7233	20.00(5)	2700	1600.0(5)
13	0.7194	21.00(5)	3200	1600.0(5)
14	0.6778	22.00(5)	4000	1600.0(5)
15	0.7202	23.00(5)	3500	1600.0(5)

itself, experience inelastic scattering and bring ^{115}In to an isomeric state. By tracking the events in the described simulation, where the sample was exposed to a photon beam at a distance of 136 cm, not a single such case was observed. For this reason, the simulation was repeated, with some differences in geometry: the sample was placed 20.6 cm from the tungsten converter, the diameter of the indium coin has been increased from 2 to 10 cm. In this way, the number of photons falling on the indium sample is increased by three orders of magnitude. A simulation was performed with 475×10^6 incident electrons having 23 MeV energy. It was found that out of the 41 ^{115m}In isomers, 39 of them are formed in (γ, γ') reaction and two through (n, n') reaction. For a result that would be statistically more reliable, it is necessary to perform a simulation with a larger number of incident electrons, but this result is also a good enough indication that the inelastic scattering of neutrons created in water and indium itself does not contribute more than 5% to the total activation of ^{115}In isomer state. The irradiation times and intensities of bremsstrahlung beams (the integral numbers of accelerated electrons striking tungsten target Q) are presented in Table I.

B. γ spectroscopy measurements

After the exposition, the indium coins were measured using an HPGe detector with a relative efficiency of 25% and shielded by 5 cm of lead. The irradiated indium samples were placed directly on the vertical dipstick of the detector. The time between the end of irradiation and the start of measurement varied from 34 min to 221 min, depending on the activity of the exposed indium coins and the availability of the detector.

The cooling time for the samples irradiated at high energies was longer because the activity of ^{116m}In , resulting from an increasing number of neutrons in the vicinity of the Microtron, significantly exceeded the activity of ^{115m}In and ^{113m}In . Considering that the half-life of ^{116m}In ($T_{1/2} = 54.41$ min) is

shorter than the half-lives of ^{115m}In ($T_{1/2} = 4.468$ h) and ^{113m}In ($T_{1/2} = 1.658$ h), measurements were taken after the activity of ^{116m}In had decreased to ensure low levels of dead time (up to 2%). Each indium sample was measured for a duration of 30 min, according to detector availability.

In all recorded spectra, a prominent 336.24 keV γ line, produced by the deexcitation of the isomer state of ^{115m}In , was observed. However, the γ line of ^{113m}In (391.69 keV) was very weak at low endpoint energies of the photon beam, and in some spectra, it exhibited a statistical uncertainty of up to 45%. Above 17 MeV energies, there was a rapid increase in the intensity of the 391.69 keV γ line as the $^{115}\text{In}(\gamma, 2n)^{113m}\text{In}$ reaction began to take place.

Furthermore, several strong γ lines emitted after the decay of ^{116m}In , produced by neutron capture of ^{115}In , were visible in all recorded spectra. These γ lines were used to calculate the relative detection efficiency for the applied counting geometry. The relative efficiency was obtained using a combination of exponential and second-order polynomial functions. The GENIE 2000 software was employed to extract the intensities of the observed γ lines. Parts of detected γ spectra are presented in Fig. 2.

C. Determination of relative yield

The intensities of the 336.24 keV and 391.69 keV γ lines were determined in all the recorded spectra. To obtain relative yields for all the used photon energies, Eq. (4) was applied. The results obtained from this analysis are presented in Fig. 3.

Based on the data depicted in Fig. 3, it is evident that the relative yield, as defined by Eq. (3), remains approximately constant over a wide range of energies, up to the threshold for the $^{115}\text{In}(\gamma, 2n)^{113m}\text{In}$ reaction. However, beyond this energy threshold, the yield ratio starts to increase rapidly.

In the lower-energy region, up to 17 MeV, the activity of ^{113m}In is solely attributed to the photoactivation of the isomeric state [$^{113}\text{In}(\gamma, \gamma')^{113m}\text{In}$ reaction], as described by the second term in Eq. (3). The mean value of the relative yield in the energy range from 9 MeV to 16 MeV was found to be 0.039(4).

To investigate whether this trend of the yield ratio between the photoactivation of ^{113}In and ^{115}In isomeric states persists at higher energies, TALYS 1.9 estimations of cross sections for the $^{113}\text{In}(\gamma, \gamma)^{113m}\text{In}$ and $^{115}\text{In}(\gamma, \gamma)^{115m}\text{In}$ reactions were calculated. The values of the second term in Eq. (3) were then determined for the energy range from 18 MeV to 23 MeV. Multiple models of level density were used for this test, and remarkably consistent results were obtained. For instance, with the TALYS 1.9 level density model 1 (constant temperature Fermi-gas model) and GLO (Kopecky-Uhl-generalized Lorentzian) model for the strength function, the second term in Eq. (3) varied between 0.0386 and 0.0388 in the mentioned energy range. Consequently, it can be inferred that the contribution of the second term in Eq. (3) remains constant throughout the entire energy interval depicted in Fig. 3, with the mean value of 0.039(4) serving as a reliable estimation.

The $Y(^{113m}\text{In})/Y(^{115m}\text{In})$ ratio was corrected using this value, and subsequently, the analysis focused on the first term in Eq. (3). In this simplified form, the corrected yield

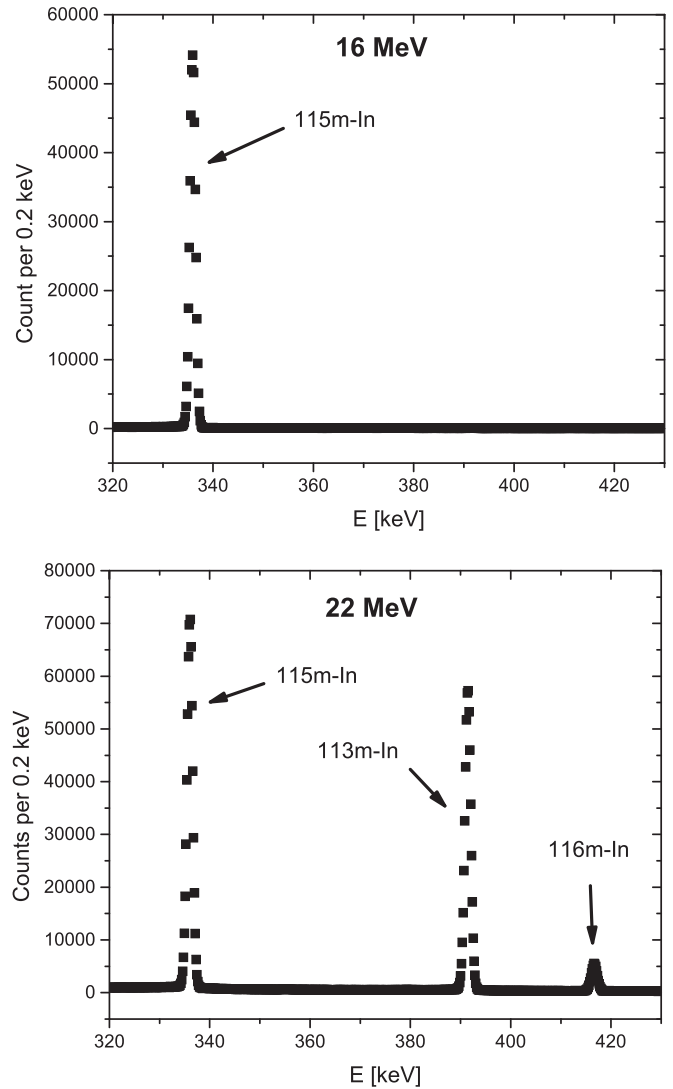


FIG. 2. Part of the γ -ray spectra collected after irradiation with 16 MeV and 22 MeV beams. The γ lines of interested are labeled. Energy width of one channel is 0.2 keV.

ratio reduces to the ratios of the saturation activities of the $^{115}\text{In}(\gamma, 2n)^{113m}\text{In}$ and $^{115}\text{In}(\gamma, \gamma')^{115m}\text{In}$ reactions.

D. Determination of photon flux

The calculation of relative yield Eq. (1) require knowing of bremsstrahlung photon spectra. For that purpose Monte Carlo (MC) simulations were used.

To estimate the flux of incident photons $\Phi(E)$ for the six used energies we employed GEANT4 (G4) version 11.01.p02 [10] with the experimental physics list QBBC. QBBC uses the standard G4 electromagnetic physics option without optical photon simulations and, the hadronic part of this physics list consists of elastic, inelastic, and capture processes. Each hadronic process is built from a set of cross sections and interaction models, which provide the detailed physics implementation. The simulated photon spectra are depicted in Fig. 4.

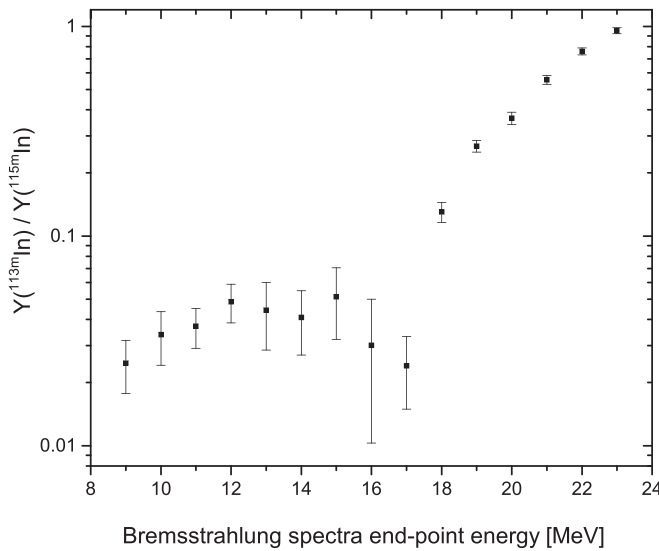


FIG. 3. Experimentally obtained relative yields $\frac{Y(^{113m}\text{In})}{Y(^{115m}\text{In})}$ for certain values of bremsstrahlung spectra end-point energy.

IV. RESULTS AND DISCUSSION

As it was mentioned in Sec. II, the set of obtained experimental data gives us two possibilities: (i) to check whether the theoretical and experimental cross-section values of the observed photonuclear reactions can reproduce the obtained results of measurement and (ii) to reconstruct the cross section for $^{115}\text{In}(\gamma, 2n)^{113m}\text{In}$ reaction.

A. Comparison of measured yield ratios with calculated ones

In the analysis of Eq. (3), we had the advantage of utilizing multiple data sets:

- (1) Results obtained from TALYS 1.9 calculations for $\sigma_{\gamma,\gamma}^{115}$ and $\sigma_{\gamma,2n}^{115}$.

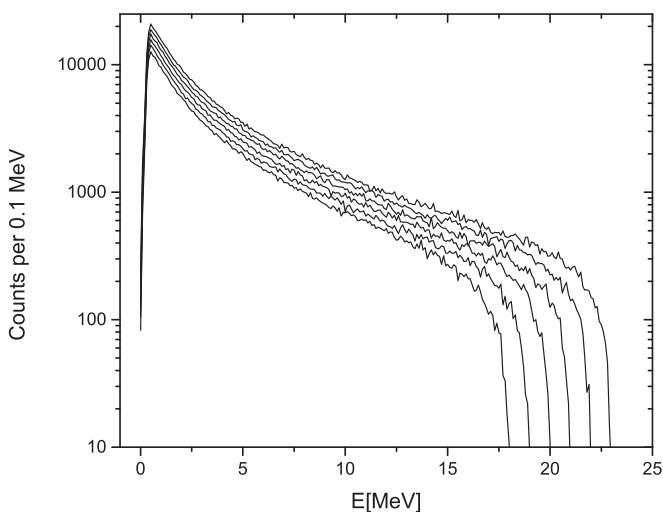


FIG. 4. Spectra of photon flux on the indium disks for electrons energies between 18 MeV and 23 MeV incident on the tungsten radiator. The electron energy corresponds to the end-point energy of the respective photon-flux spectrum (E_{max} in the Table I.)

- (2) Experimentally derived cross section for the $^{115}\text{In}(\gamma, 2n)^{113m}\text{In}$ reaction.
- (3) Several measured cross sections for the photoactivation of ^{115m}In .

1. $\sigma_{\gamma,\gamma}^{115}$ and $\sigma_{\gamma,2n}^{115}$ estimated by TALYS 1.9

For the first check, TALYS 1.9 estimates of the cross sections of the observed reactions were chosen to be used. There were employed two different strength function models, and for each of them, cross sections for all six models describing the level density available in TALYS 1.9 were calculated. Available level density models in the TALYS 1.9 are [11–19]:

- (1) LD model 1: the constant temperature Fermi-gas model;
- (2) LD model 2: the back-shifted Fermi-gas model;
- (3) LD model 3: the generalized superfluid model;
- (4) LD model 4: the microscopic level densities based on the Goriely's tables;
- (5) LD model 5: Hilaire's combinatorial tables;
- (6) LD model 6: the temperature-dependent Hartree-Fock-Bogoliubov model, Gogny force.

The first cross-section estimation was performed using the GLO model for the radiation strength function, just as recommended in Ref. [20]. The reliability of the obtained results was checked by comparing the TALYS 1.9 results with the experimentally derived cross section of the $^{115}\text{In}(\gamma, \gamma')^{115m}\text{In}$ reaction. In this way, different models of the level density yield small differences in the cross section, but for all of them, it is common that the maximum value of the cross section is at 9.2 MeV, while the maximum value in the peak ranges from 0.865 mbarn to 1.14 mbarn. In most of the experimental results, the value of the cross section in the peak is around 1 mbarn. However, in Ref. [20], after careful measurements and calculation, it is obtained that the maximum value of the cross section could exceed 3 mbarn if some other model for the radiation strength function was chosen. For this reason, the decision was made to perform the calculations with cross sections obtained using another model of the strength function, which gives cross sections with a maximum value of around 3 mbarn. The Brink-Axel Lorentzian strength function (BAL) was used. In this case, the maximum cross-section value is at 9.2 MeV, and six different models of level density give peak values in the range from 2.96 mbarn to 3.66 mbarn. Six cross sections obtained using the GLO model and six cross sections obtained using the BAL model for the strength function are presented in Fig. 5.

The procedure was completely repeated for the $^{115}\text{In}(\gamma, 2n)^{113m}\text{In}$ reaction. Both the GLO and BAL strength function models were chosen, and for each of them, the cross sections with all six level density models were calculated. The results obtained are presented in Fig. 6.

From the graphical representation of the TALYS 1.9 cross section, it can be observed that there is a certain scatter in the shape of the function. However, unlike the case of the $^{115}\text{In}(\gamma, \gamma')^{115m}\text{In}$ reaction, no distinct separation into two clearly separated groups can be seen. The only existing measured cross section for this reaction [5] is depicted by the

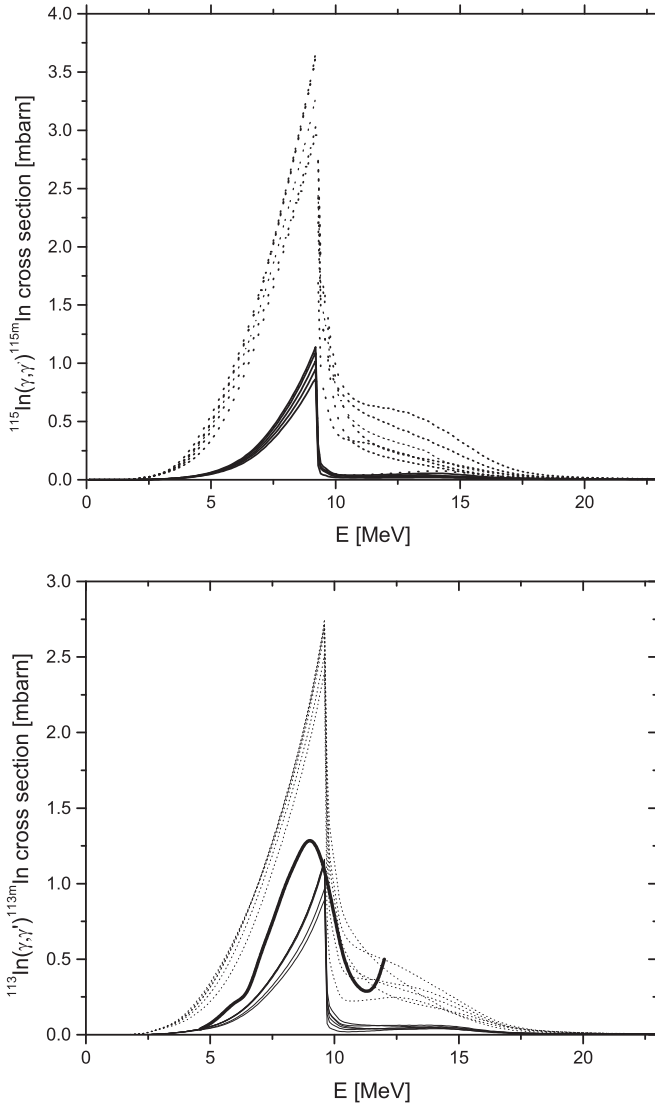


FIG. 5. The above graph: TALYS 1.9 calculation of cross sections for $^{115}\text{In}(\gamma, \gamma')^{115m}\text{In}$ reaction obtained using the GLO (solid line) and BAL (dotted line) models for radiation strength function and six models for level density. Bottom graph: TALYS 1.9 calculation of cross sections for $^{113}\text{In}(\gamma, \gamma')^{113m}\text{In}$ reaction obtained using the GLO (thin solid line) and BAL (dotted line) models for radiation strength function and six models for level density; thick line: experimental data with spline interpolation [21].

thick solid line in Fig. 6. A notable observation is that the measured cross-section values significantly differ from the cross sections obtained by TALYS 1.9 calculation.

The integrals (saturation activities) in the first term of Eq. (3) were calculated for several endpoint energies ranging from 18 MeV to 23 MeV using the obtained cross sections and G4 photon flux simulations. For each observed energy, six estimates for cross sections (and consequently, six values of saturation activities) were obtained for both the $(\gamma, 2n)$ and (γ, γ') reactions using one chosen model of the strength function.

Each saturation activity value obtained using one strength function model, for the $(\gamma, 2n)$ reaction was combined with

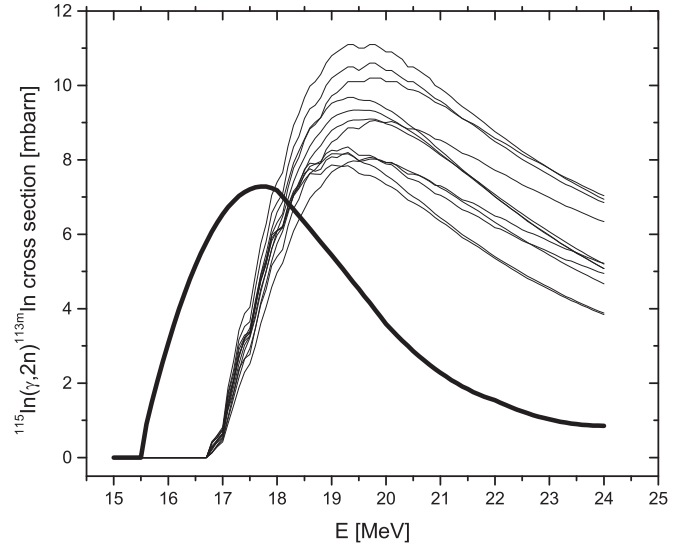


FIG. 6. Thin line: TALYS 1.9 calculation of cross sections for $^{115}\text{In}(\gamma, 2n)^{113m}\text{In}$ reaction obtained using the GLO and BAL models for radiation strength function and six models for level density; thick line: experimental data from Ref. [5].

each value for the (γ, γ') reaction, resulting in 36 estimates for one observed energy. The same procedure was repeated for a second model of the strength function, leading to another 36 combinations of saturation activity ratios. The outcomes of these calculations are presented in Fig. 7. At first glance, it can be seen that the obtained results of $Y(^{113m}\text{In})/Y(^{115m}\text{In})$ yield ratio are grouped into two bands, each obtained using one strength function. The upper band is obtained using GLO strength function model, while BAL model gives the lower cluster.

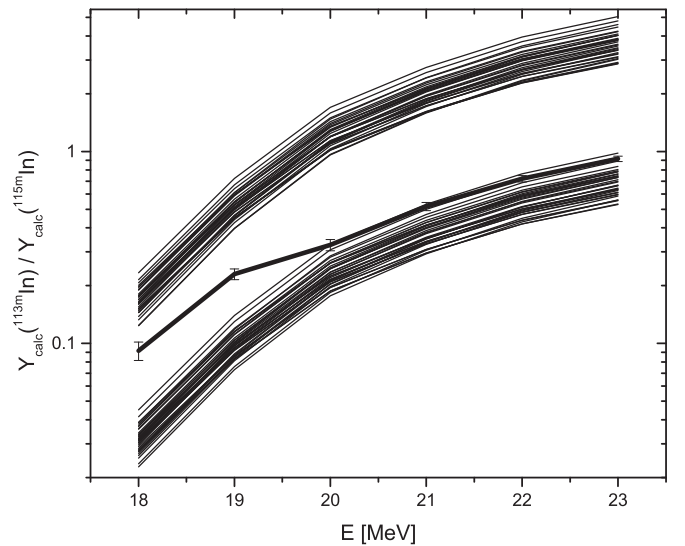


FIG. 7. Comparison of calculated yields $Y(^{113m}\text{In})/Y(^{115m}\text{In})$ using TALYS 1.9 results with measured ones presented by thick solid line. The top band consisting of 36 values of the $Y(^{113m}\text{In})/Y(^{115m}\text{In})$ yield ratio was obtained with the GLO model, while the bottom band contains yield values calculated using the BAL model.

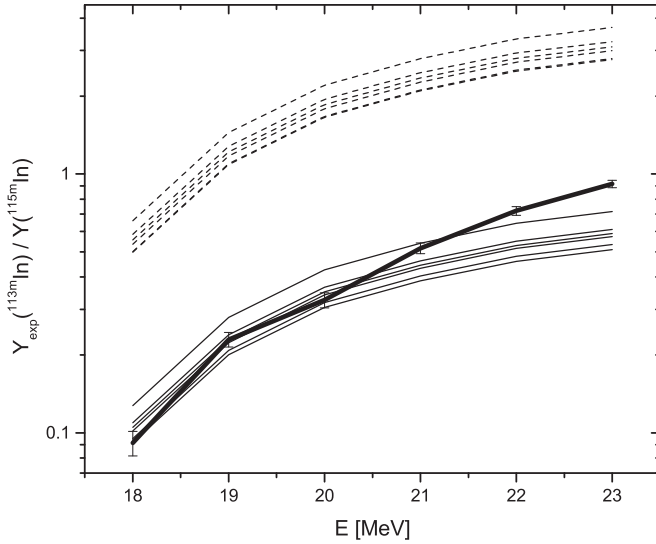


FIG. 8. Comparison of calculated yield ratios $Y(^{113m}\text{In})/Y(^{115m}\text{In})$ using TALYS 1.9 results available and experimental data [5] with measured ones. Top band is obtained using GLO model while the bottom one is calculated using BAL model.

It is important to note that the lines in Fig. 7, are provided solely as visual aids and do not result from a fit. The experimental results are represented by points and a thick line.

2. TALYS estimate for $\sigma_{\gamma,\gamma}^{115}(E)$ and experimentally determined $\sigma_{\gamma,2n}^{115}(E)$

Available data for the $^{115}\text{In}(\gamma, 2n)^{113m}\text{In}$ reaction cross section $\sigma_{\gamma,2n}^{115}(E)$ can be found in Ref. [5]. The saturation activities of this reaction were calculated for several endpoint energies from 18 MeV to 23 MeV of the using these cross section and reconstructed photon spectra $\Phi(E)$. Calculations of $\sigma_{\gamma,\gamma}^{115}(E)$ were performed using two different models of strength function, and all six models for level densities. For both groups of six cross section estimates, saturation activities were calculated, in the range between 18 MeV and 23 MeV. Ratios of saturation activities were calculated and obtained values are compared with experimentally derived values in Fig. 8. Thick solid line connects experimentally derived values $Y(^{113m}\text{In})/Y(^{115m}\text{In})$ ratios of reaction yields. Thin solid lines are obtained using GLO model of strength function, while thin dotted lines represent ratios of saturation activities calculated using cross sections estimated using BAL strength function model. Considering that two groups of cross sections for $\sigma_{\gamma,\gamma}^{115}(E)$ reactions differ significantly in amplitude depending on chosen model of strength function, as can be seen from Fig. 5, calculated ratios of reaction yields $Y(^{113m}\text{In})/Y(^{115m}\text{In})$ are grouped in two separated clusters.

3. Experimentally determined both $\sigma_{\gamma,\gamma}^{115}(E)$ and $\sigma_{\gamma,2n}^{115}(E)$

Although there are several published results of measurements of the cross section for the $^{115}\text{In}(\gamma, \gamma')^{115m}\text{In}$ reaction, none of them fully satisfy the requirements of this study. The primary reason is that the cross sections for the mentioned reaction were not measured across a sufficiently wide energy

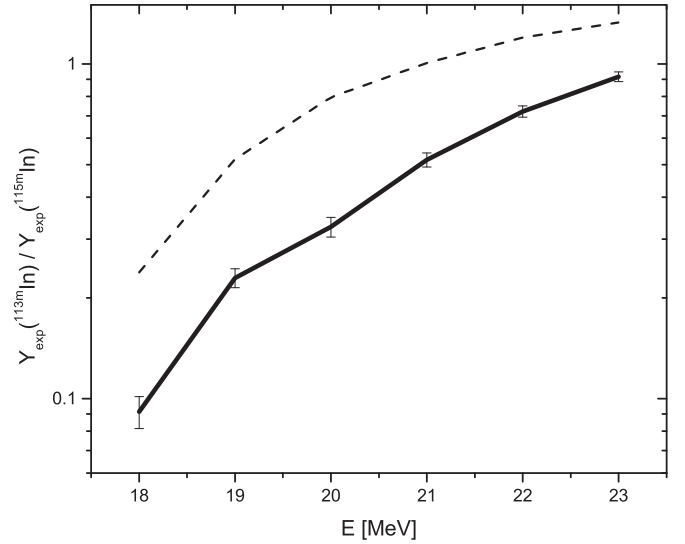


FIG. 9. Comparison of calculated yield ratios $Y(^{113m}\text{In})/Y(^{115m}\text{In})$ using available experimental data for the $^{115}\text{In}(\gamma, \gamma')^{115m}\text{In}$ reaction [22] and $^{115}\text{In}(\gamma, 2n)^{113m}\text{In}$ reaction [5] with measured ones. Results of calculations are connected by dashed line.

range. The only paper presenting cross-section results at high energies [5] was rejected due to unrealistically high values of the cross section in the 20 MeV region. Consequently, the decision was made to utilize the cross sections published in Ref. [22], which demonstrate a reasonable agreement with the TALYS 1.9 estimates.

However, it should be noted that the main limitation of this data set is that the cross sections are only determined up to a maximum energy of 12 MeV. To accommodate the analysis, it is assumed that the cross-section values in the energy interval from 12 MeV to 23 MeV are not significantly large. Under this assumption, the absence of data in the high-energy region would not have a substantial impact on the value of the saturation activity. Figure 5 reveals that GLO model used for calculating the TALYS 1.9 cross section predicts a very small value of the cross section in the high-energy area.

Similarly, the saturation activity for the $^{115}\text{In}(\gamma, 2n)^{113m}\text{In}$ reaction was calculated using the experimental cross-sectional values published in Ref. [5]. The calculated values of the yield ratio are then compared with the experimental data in Fig. 9.

B. Cross section of $^{115}\text{In}(\gamma, 2n)^{113m}\text{In}$ reaction obtained by unfolding procedure

In this study, we applied the unfolding technique to obtain a more suitable cross section for the $^{115}\text{In}(\gamma, 2n)^{113m}\text{In}$ reaction in the energy range from the reaction threshold up to 23 MeV. To derive the unfolding values of the phase cross section, the Eq. (3) was transformed as follows:

$$\begin{aligned} A_k &= \frac{Y(^{113m}\text{In})}{Y(^{115m}\text{In})} \cdot \int_{E_{th}^{\gamma,\gamma}}^{E_{max_k}} \sigma_{\gamma,\gamma}^{115}(E) \Phi(E)_k dE \\ &= \int_{E_{th}^{\gamma,2n}}^{E_{max_k}} \sigma_{\gamma,2n}^{115}(E) \Phi(E)_k dE, \end{aligned} \quad (5)$$

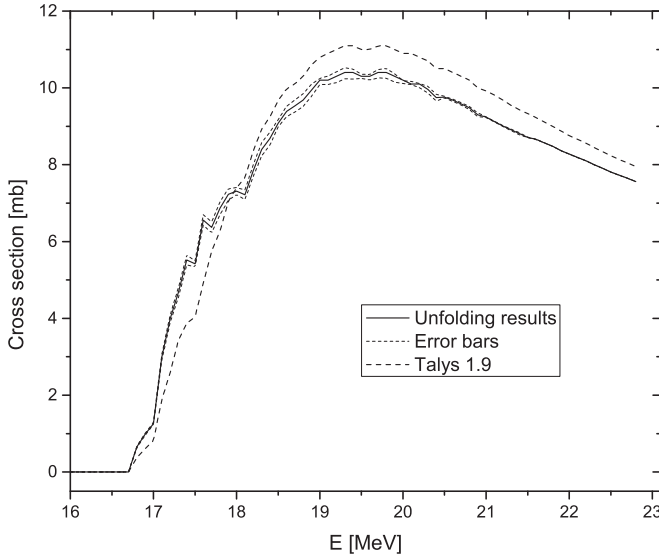


FIG. 10. Unfolded results for the $^{115}\text{In}(\gamma, 2n)^{113m}\text{In}$ cross section (line with a corridor of uncertainty) in comparison with default TALYS 1.9 function.

where the index k indicates the number of the irradiated disk and in this case it goes from 1–6 for six activated energies.

For the unfolding process, the input quantities included $A_k = Y_k(^{113m}\text{In})/Y_k(^{115m}\text{In}) \cdot \int_{E_{th}^{\gamma,\gamma'}}^{E_{max,k}} \sigma_{\gamma,\gamma'}^{115}(E)\Phi(E)_k dE$ [saturation activity of $^{115}\text{In}(\gamma, \gamma')^{115m}\text{In}$ multiplied by experimentally determined reaction yields]. In Eq. (5), A_k was calculated using the values of the cross section function for the $^{115}\text{In}(\gamma, \gamma')^{115m}\text{In}$ reaction obtained by TALYS 1.9 calculations using model 6 for level density and BAL model for radiation strength function. This specific model combination was selected as it demonstrated the best agreement with experimentally determined yields (Fig. 7).

Similarly, in the unfolding procedure for the $^{115}\text{In}(\gamma, 2n)^{113m}\text{In}$ reaction, the starting default function utilized TALYS 1.9 calculations with model 3 for level density and BAL for radiation strength function, as this combination also provided the best agreement with experimental results (Fig. 7). The unfolding procedure employed the MAXED algorithm [23], which utilizes input data of measured induced specific saturated activity A_k to derive a function $\sigma(E)$ maximizing the relative entropy S , defined as follows:

$$S = - \int \left(\sigma(E) \ln \left(\frac{\sigma(E)}{\sigma_{\text{def}}(E)} \right) + \sigma_{\text{def}}(E) - \sigma(E) \right) dE. \quad (6)$$

Here, $\sigma_{\text{def}}(E)$ represents the default cross-section function.

Unfolding procedures were conducted within the energy range of 16 MeV to 22.8 MeV, which was divided into 71 bins. The result obtained by employing the MAXED algorithm is depicted in Fig. 10. Corridor of uncertainty was calculated by MAXED algorithm and included influence of uncertainty of A to final cross-section values.

To validate the unfolding results, an induced activity $[A_{kc} = \sum \sigma(E_i) \cdot \Phi(E_i) \cdot \Delta E]$ was calculated and then compared with the measured data. This comparison was performed for default cross-section functions and the MAXED

results and the sum of the squared of relative deviation σ is calculated as:

$$S = \frac{1}{(k-1)} \sum_1^k \sigma^2 = \frac{1}{(k-1)} \sum_1^k \left(\frac{A_{kc} - A_{ke}}{A_{ke}} \right)^2. \quad (7)$$

The obtained values are $S = 0.13$ for the default spectrum and $S = 0.08$ for the unfolding results. This indicates that the unfolding outcomes provide a better description of the measured experimental data compared to the TALYS 1.9 calculations.

V. DISCUSSION

The first check was conducted by utilizing the cross-section values obtained by the TALYS 1.9 code for both reactions, $^{115}\text{In}(\gamma, 2n)^{113m}\text{In}$ and $^{115}\text{In}(\gamma, \gamma')^{115m}\text{In}$. Each estimate for the $^{115}\text{In}(\gamma, 2n)^{113m}\text{In}$ reaction was combined with each estimate obtained for the $^{115}\text{In}(\gamma, \gamma')^{115m}\text{In}$ reaction, resulting in 36 distinct values for the saturation activity ratios for a specific strength function choice.

It is evident that the 36 combinations of saturation activity ratios are grouped into two clusters. The lower cluster was obtained using the BAL radiation strength function, which provides higher cross-section values for the $^{115}\text{In}(\gamma, \gamma')^{115m}\text{In}$ reaction, approximately around 3 mbarn. Notably, at energies of 20 MeV and above, the highest estimated ratios of saturation activities align closely with the experimental results. However, at energies below 20 MeV, the experimental values slightly exceed the values obtained based on TALYS 1.9 sections.

On the other hand, the upper cluster comprises 36 combinations of saturation activity ratios obtained using the GLO model for the radiation strength function. It is evident that lower estimations of cross sections for the $^{115}\text{In}(\gamma, \gamma')^{115m}\text{In}$ reaction, around 1 mbarn, lead to overestimated values of the yield ratio.

In summary, the analysis of these saturation activity ratios obtained through different radiation strength function models indicates that the BAL model tends to yield better agreement with experimental data at higher energies, while the GLO model tends to overestimate the yield ratio due to lower estimations of the cross sections for the $^{115}\text{In}(\gamma, \gamma')^{115m}\text{In}$ reaction. If we focus on the energy region higher than 20 MeV, it can be observed that of the 36 TALYS combinations there are some that show good agreement with the experiment. It can be observed that the best agreement with the experiment is given by the combination in which the cross section for $^{115}\text{In}(\gamma, 2n)^{113m}\text{In}$ reaction is calculated using LD model 3 (the generalized superfluid model) and cross section of $^{115}\text{In}(\gamma, \gamma')^{115m}\text{In}$ reaction is estimated using LD model 6 (the temperature-dependent Hartree-Fock-Bogoliubov model, Gogny force).

In the second scenario, where one experimentally established cross section was available in the databases for the $^{115}\text{In}(\gamma, 2n)^{113m}\text{In}$ reaction, the comparison with the experimental results yielded similar outcomes. Notably, the cross section for the $^{115}\text{In}(\gamma, \gamma')^{115m}\text{In}$ reaction, calculated using the GLO radiation strength function in all six subvariants obtained by choosing the level density function, exhibited

significantly higher values of the saturation activity ratio compared to the measured values. The estimated ratios of saturation activities were found to be larger than the experimental ones when using cross sections for the $^{115}\text{In}(\gamma, 2n)^{113m}\text{In}$ reaction, which have maximum values around 1 mbarn.

Of particular interest was the comparison of the experimental values of the $Y(^{113m}\text{In})/Y(^{115m}\text{In})$ yield ratio with the calculated values when employing the BAL radiation strength function to estimate the cross section of the $^{115}\text{In}(\gamma, \gamma')^{115m}\text{In}$ reaction. Remarkably, a much better agreement with the experimental data was achieved in this case. Figure 6 clearly illustrates that the experimental value of the cross section for the $^{115}\text{In}(\gamma, 2n)^{113m}\text{In}$ reaction has a lower threshold compared to the prediction from TALYS 1.9 calculations. Consequently, the saturation activity calculated using this cross section increases more rapidly with increasing energy than the saturation activities obtained using the TALYS 1.9 cross sections for the same reaction in energy region up to 20 MeV. For this reason, it can be seen in Fig. 8 that the measured and calculated values of $Y(^{113m}\text{In})/Y(^{115m}\text{In})$ yield ratio coincide at lower energies, while the difference is observed at energies higher than 20 MeV. However, as the experimental cross section decreases significantly faster in high-energy region, compared to the TALYS 1.9 cross section, the ratio of saturation activities shows a slower increase with increasing energy. This effect is evident in Fig. 8, where the experimental values of the ratio of saturation activities at energies above 20 MeV are higher than the calculated ones.

In Fig. 9, it is evident that when calculating the ratio of saturation activities using experimentally established cross sections for both reactions, the obtained values significantly exceed the values measured in this experiment. This outcome was anticipated, as the cross section utilized for the $^{115}\text{In}(\gamma, \gamma')^{115m}\text{In}$ reaction has values similar to those obtained using the GLO model for the radiation strength function.

It was shown that, based on the measured $Y(^{113m}\text{In})/Y(^{115m}\text{In})$ yield ratio values, the unfolding technique can be used to estimate the energy differential cross section for the $^{115}\text{In}(\gamma, 2n)^{113m}\text{In}$ nuclear reaction. The resulting estimate is shown in Fig. 10. This result is significantly different from the cross section shown in Ref. [5], however, it shows good agreement with the results of TALYS 1.9 calculations. Slight deviations from the smooth flow of the curve in the energy region around 18 MeV originate from some numerical effects in the unfolding procedure itself,

the most probable source of which is insufficient number and accuracy of the measured data.

VI. CONCLUSIONS

In this work, the $Y(^{113m}\text{In})/Y(^{115m}\text{In})$ yield ratio were measured in the energy interval from 18 MeV to 23 MeV, in order to verify the capacity of the existing methods for evaluating the cross section of relevant photonuclear reactions to reproduce the obtained experimental results. It was also checked whether it is possible to obtain agreement with the measured $Y(^{113m}\text{In})/Y(^{115m}\text{In})$ yield ratios with the available cross sections of the observed photonuclear reactions.

Comparisons of experimental values of $Y(^{113m}\text{In})/Y(^{115m}\text{In})$ yield ratio with the results of calculations based on TALYS 1.9 evaluated cross sections, showed that the best agreement is obtained if the cross section of $^{115}\text{In}(\gamma, \gamma')^{115m}\text{In}$ reactions is calculated in the way suggested in Ref. [20]. This raises the need to carefully check the cross section for $^{115}\text{In}(\gamma, \gamma')^{115m}\text{In}$ reaction, since most of the so far known measurements give lower values of the cross section than suggested in Ref. [20]. However, it was shown in this experiment that those lower cross section values for the $^{115}\text{In}(\gamma, \gamma')^{115m}\text{In}$ reaction, good agreement with the measured $Y(^{113m}\text{In})/Y(^{115m}\text{In})$ yield ratios is not obtained.

Based on cross sections for a given reaction, estimated using TALYS 1.9, $Y(^{113m}\text{In})/Y(^{115m}\text{In})$ yield ratios were and compared with measured ones. This study shows that the best agreement with the experimental data is obtained when the cross sections for the $^{115}\text{In}(\gamma, 2n)^{113m}\text{In}$ reaction is estimated using generalized superfluid model for the level density calculation, and temperature-dependent Hartree-Fock-Bogoliubov model, Gogny force model for $^{115}\text{In}(\gamma, \gamma')^{115m}\text{In}$ reaction. In both cases the BAL model of the radiation strength function is recommended. However, these results should only be conditionally accepted since there is a certain deviation between the experimental and calculated $Y(^{113m}\text{In})/Y(^{115m}\text{In})$ yield ratio values at lower energies.

Also in this paper, the estimation of cross sections for $^{115}\text{In}(\gamma, 2n)^{113m}\text{In}$ reaction was performed using the unfolding method. The first results are encouraging and in much better agreement with the cross sections obtained by TALYS 1.9 calculations than the only cross section for this reaction that can be found in the literature. There is room to better determine this cross section in repeated measurements where the saturation activities would be determined for a larger number of energies in the energy interval of interest.

-
- [1] A. Zilges, D. Balabanski, J. Isaak, and N. Pietralla, *Prog. Part. Nucl. Phys.* **122**, 103903 (2022).
- [2] T. Kawano, Y. Cho, P. Dimitriou, D. Filipescu, N. Iwamoto, V. Plujko, X. Tao, H. Utsunomiya, V. Varlamov, R. Xu, R. Capote, I. Gheorghe, O. Gorbachenko, Y. Jin, T. Renstrøm, M. Sin, K. Stopani, Y. Tian, G. Tveten, J. Wang *et al.*, *Nucl. Data Sheets* **163**, 109 (2020).
- [3] S. S. Dietrich and B. L. Berman, *At. Data Nucl. Data Tables* **38**, 199 (1988).
- [4] A. Koning and D. Rochman, *Nucl. Data Sheets* **113**, 2841 (2012), special Issue on Nuclear Reaction Data.
- [5] O. Bogdankevich, L. Lazareva, and F. Nikolaev, *J. Exp. Theor. Phys.* **4**, 320 (1957).
- [6] M. Erhard, A. R. Junghans, R. Beyer, E. Grosse, J. Klug, K. Kosev, C. Nair, N. Nankov, G. Rusev, K. D. Schilling, R. Schwengner, and A. Wagner, *Eur. Phys. J. A* **27**, 135 (2006).
- [7] Janis nuclear data, https://www.oecd-nea.org/jcms/pl_39910/janis.

- [8] 25-microtron, <http://flerovlab.jinr.ru/mt-25-microtron/>.
- [9] M. Krmar, Y. Teterev, A. Belov, and S. Mitrofanov, *Nucl. Instrum. Meth. Phys. Res. A* **901**, 133 (2018).
- [10] S. Agostinelli, J. Allison, K. Amako, J. Apostolakis, H. Araujo, P. Arce, M. Asai, D. Axen, S. Banerjee, G. Barrant, F. Behner, L. Bellagamba, J. Boudreau, L. Broglia, A. Brunengo, H. Burkhardt, S. Chauvie, J. Chuma, R. Chytracek, G. Cooperman *et al.*, *Nucl. Instrum. Meth. Phys. Res. A* **506**, 250 (2003).
- [11] A. Koning and J. Delaroche, *Nucl. Phys. A* **713**, 231 (2003).
- [12] W. Hauser and H. Feshbach, *Phys. Rev.* **87**, 366 (1952).
- [13] C. Kalbach, *Phys. Rev. C* **33**, 818 (1986).
- [14] A. Gilbert and A. Cameron, *Can. J. Phys.* **43**, 1446 (1965).
- [15] W. Dilg, *Nucl. Phys. A* **217**, 269 (1973).
- [16] A. Zubov, G. Adamian, and N. Antonenko, *Phys. Part. Nucl.* **40**, 847 (2009).
- [17] A. V. Ignatyuk, J. L. Weil, S. Raman, and S. Kahane, *Phys. Rev. C* **47**, 1504 (1993).
- [18] S. Goriely, S. Hilaire, and A. J. Koning, *Phys. Rev. C* **78**, 064307 (2008).
- [19] S. Hilaire, M. Girod, S. Goriely, and A. J. Koning, *Phys. Rev. C* **86**, 064317 (2012).
- [20] M. Versteegen, D. Denis-Petit, V. Méot, T. Bonnet, M. Comet, F. Gobet, F. Hannachi, M. Tarisien, P. Morel, M. Martini, and S. Péru, *Phys. Rev. C* **94**, 044325 (2016).
- [21] Z. M. Bigan, V. A. Zheltonozhsky, V. I. Kirishchuk, V. M. Mazur, D.N.Simochko, and P.N.Trifonov, *Bull. Russ. Acad. Sci. - Phys.* **70**, 292 (2006).
- [22] V. Mazur, I. Sokolyuk, Z. Bigan, and I. Kobal, *Phys. At. Nucl.* **56**, 10 (1993).
- [23] M. Reginatto and P. Goldhagen, *Health Phys.* **77**, 579 (1999).